RSC Advances

PAPER

View Article Online
View Journal | View Issue

Cite this: *RSC Adv.*, 2026, **16**, 24933

Evaluating the combined effect of a biomimetic organic matrix and bioinspired fluorapatite nanoparticles on initial caries lesions

Rehab M. El-Sharkawy, *[a] Rania A. Hanafy,[bc] Wafaa Yahia Alghonemy,[d] Omnia M. Abdelfatah[e] and Eman M. Salem[e]

This study found that combining a biomimetic organic matrix of chitosan (CS) and carboxymethyl cellulose (CMC) with bioinspired fluorapatite nanoparticles (Nano-FA) significantly enhanced the remineralization of early enamel caries lesions. A total of 40 extracted third molars were sectioned into 200 enamel specimens and randomly allocated into five groups: sound enamel (baseline), demineralized enamel, CS-treated, Nano-FA-treated, and CS-Nano-FA-CMC-treated groups. Remineralization efficacy was assessed using Vickers microhardness testing, scanning electron microscopy (SEM), and energy-dispersive X-ray (EDX) analysis. Among all evaluated groups, both Nano-FA and CS-Nano-FA-CMC treatments notably improved enamel microhardness, restoring values close to those of sound enamel. The CS-Nano-FA-CMC group displayed pronounced mineral deposition on the enamel surface and a markedly higher Ca/P ratio ($p < 0.001$) than other groups. These findings indicate that the CS-Nano-FA-CMC composite is especially effective at promoting remineralization, likely due to synergistic action that results in sustained release of calcium, phosphate, and fluoride ions, and facilitates apatite formation. Within the limitations of this *in vitro* study, the developed nanocomposite demonstrates strong potential as a future biomimetic agent for managing early enamel caries lesions.

Received 19th March 2026
Accepted 8th May 2026

DOI: 10.1039/d6ra02288j

rsc.li/rsc-advances

1 Introduction

Dental caries is a worldwide oral disease caused by a complex interaction between bacteria and food debris on the tooth surface. Bacteria metabolize food debris for energy and produce acid as a byproduct; this acid causes damage to the enamel.[1] Under SEM, enamel appears as a highly mineralized tissue composed of nano-rod hydroxyapatite crystals. Demineralization is the *in vivo* dissolution of calcium phosphate minerals from the hydroxyapatite lattice.[2] Moreover, decreased salivary secretion compromises both the buffering capacity and the supply of essential phosphate and calcium ions, thereby weakening the body's natural remineralization process, which is inherently equipped to balance demineralization. Together, these factors contribute to progressive enamel demineralization, leading to white spot lesions. If left untreated, it will lead to cavitation.[3,4]

Enamel, despite being the hardest tissue in the human body, lacks inherent regenerative ability, making its repair a persistent challenge in restorative dentistry. Despite this limitation, appropriate conditions, if provided, can shift the process towards remineralization, thus healing the lesion. Conventionally, this process has been promoted primarily through the application of fluoride-based agents as a gold standard.[5]

Although fluoride encourages mineral deposition at the start of the remineralization process, its action often reaches a limit and does not fully restore the original enamel architecture.[6] Concerns have also been raised about long-term systemic exposure, as higher intake, especially in fluoridated regions, has been associated with a greater risk of dental fluorosis.[7] These issues have motivated researchers to explore alternative materials that do not rely on fluoride yet still support true enamel regeneration. Current efforts focus on calcium phosphate-based materials, particularly amorphous calcium phosphate (ACP), as they provide a direct source of ions for crystal formation. Other strategies include the use of bioactive glasses that release mineralizing ions capable of initiating apatite formation, and peptide systems that mimic enamel matrix proteins and guide crystal organization. Together, these emerging approaches offer a biomimetic pathway for rebuilding enamel that may achieve outcomes beyond what fluoride alone can provide.[8,9]

[a]*Chemistry Department, Faculty of Dentistry, Pharos University in Alexandria, P.O. Box 37, Sidi Gaber, Alexandria, Egypt. E-mail: rehab.mansour@pua.edu.eg; Tel: +0020-01229727752*

[b]*Dental Materials Department, Faculty of Dentistry, Pharos University in Alexandria, P.O. Box 37, Sidi Gaber, Alexandria, Egypt*

[c]*Dental Materials Department, Faculty of Dentistry, Alexandria University, Alexandria Main University Hospital, Alexandria, Egypt*

[d]*Oral Biology Department, Faculty of Dentistry, Tanta University, Tanta, Egypt*

[e]*Oral Biology Department, Faculty of Dentistry, Pharos University in Alexandria, P.O. Box 37, Sidi Gaber, Alexandria, Egypt*

In recent years, biomimetic mineralization has emerged as a promising strategy, inspired by the natural process of enamel formation known as amelogenesis.[10] A cell-free strategy focuses on reproducing the natural events that guide enamel formation, particularly the organization and mineralization stages seen during amelogenesis. The organic matrix plays a central role here; the maestro is amelogenin, which guides the ordered deposition of hydroxyapatite crystals. To imitate this biological guidance system, researchers have turned to a range of natural and synthetic biopolymers and investigated their ability to regulate apatite nucleation, growth, and maturation.

One of the most promising materials is chitosan (CS), a positively charged biopolymer derived from chitin. Its cationic nature allows it to bind to areas of defective enamel that have lost minerals. Once attached, CS can attract calcium and phosphate ions from the surrounding environment, thereby providing a localized template for the development of new hydroxyapatite crystals.[11,12] Through this combination of surface affinity and nucleating agent, CS functions as a supportive scaffold for biomimetic enamel formation.

Nanohydroxyapatite (Nano-HA) has been introduced as a nanotechnology-based method for enamel regeneration. Due to its structural and compositional similarity to natural apatite, Nano-HA can integrate with existing enamel crystallites and facilitate the deposition of a synthetic apatite layer over demineralized areas, thus enhancing mineral density and surface microhardness.[13] Evidence indicates that the demineralizing effect is primarily restricted to the outer enamel layer, with minimal penetration into subsurface lesions, thus limiting its capacity for complete lesion reversal.[14] Fluorahydroxyapatite (FHA) exhibits improved characteristics; however, fluorapatite (FA) has garnered considerable attention due to its superior stability, acid resistance, and efficacy in remineralization.[15] Nonetheless, like fluoride, their effectiveness may be constrained by insufficient retention on enamel surfaces and the lack of a structural matrix to facilitate crystal growth organization.[16] Recent advances in enamel regeneration highlight a divide between two main strategies: the first strategy aims at using synthetic material and imprinting it with the composition, morphology, and physico-chemical properties of the biogenic material, and the other strategy is to find and develop analogs of the natural enamel protein (amelogenin) to imitate the natural process of enamel formation.

This study introduces a novel composite formulation that combines nanotechnology and biomimetic principles, recognizing the limitations of employing either biomimetic scaffolds, such as chitosan (CS), or nanotechnology-based fillers, such as fluorapatite nanoparticles (Nano-FA), independently. A synergistic composite can be created by integrating the biological recognition and enamel-binding properties of CS with Nano-FA's enhanced remineralization capabilities. This composite unites them on a carboxymethyl cellulose (CMC) foundation. CMC enhances the workability and structural integrity of dental composites. CMC also provides an adhesive surface that can interact directly with enamel irregularities, improving its ability to bind and remain in place during treatment. Because of these properties, CMC has become an important element in many modern restorative formulations.[17,18] When combined with chitosan, the electrostatic attraction between the two polymers produces a cohesive, gel-like network. This matrix improves handling and stability, enabling active agents to be delivered more precisely.[19] This research introduces a CS-Nano-FA-CMC composite that combines biomimetic scaffolding with bioinspired nanoscale mineral components and a functional polymeric matrix, potentially improving enamel remineralization treatment methods.

2 Materials & methods

This study complied with the regulations established by the Faculty of Pharmacy Research Ethics Committee at Pharos University in Alexandria, as specified by Ethical Code #PUA022025083388. All procedures involving the use of extracted human teeth were conducted in accordance with the Declaration of Helsinki and institutional protocols, and received approval from the local ethics committee after informed consent was obtained from all donors.[20]

2.1 Materials

CS used in this study, obtained from Sigma-Aldrich, exhibits an average molecular weight ranging from 190 to 310 kDa, with a degree of deacetylation between 75% and 85%, and a viscosity of 200–800 cP when measured as a 1 wt% solution in 1% acetic acid at 25 °C using a Brookfield viscometer. Calcium nitrate tetrahydrate ($Ca(NO_3)_2$ $4H_2O$, FW 236.15 g mol^{-1}, assay of ≥ 99.0%) was purchased from Sigma Aldrich, USA. Methanol ($CH_{33}OH$, FW 32.04 g mol^{-1}, assay 99.8%), potassium chloride (KCl, FW 74.55 g mol^{-1}, assay 99.5%), and glacial acetic acid (CH_3COOH, FW 60.05 g mol^{-1}, assay ≥ 99%) were sourced from BDH in the UK. Carboxymethyl cellulose (CMC) was supplied by Sigma-Aldrich, with a degree of substitution of 1.8. According to the supplier's specifications, a 1% w/v aqueous solution possesses a viscosity of 1100–1900 cP at 20 °C. Phosphorus pentoxide anhydrous (P_2O_5, FW 283.88, assay ≥ 98%), sodium hydroxide (NaOH, FW 40.0 g mol^{-1}, assay > 99%), and hexafluorophosphoric acid (HPF_6, FW 145.97, 60% w/w aqueous solution) were procured from Merck Company in Germany.

2.2 Sample size calculation

The required sample size was established using data from an earlier published study.[9] Based on results, utilizing a power of 80% ($\beta = 0.20$) to identify a standardized effect size of 0.745 in enamel remineralization (the primary outcome) and a significance level of 5% (α error accepted = 0.05), it was determined that the minimum necessary sample size is eight extracted third molars per group.[21] The current study used 40 extracted third molars. Each molar was sectioned longitudinally into five sections, and the 200 sections were randomly assigned ($n = 40$), so each tooth contributed one section per group. Any specimen excluded from the study due to processing errors will be substituted with a new one to preserve the intended sample size.[22]

2.3 Group assignment and teeth preparation

A total of 40 freshly extracted, sound human third molars were collected from patients undergoing routine surgical extractions. After the teeth were extracted, informed consent was secured from the patients for the research.[23] Teeth were required to have intact crowns, free from cracks or structural defects, and without previous restorative or endodontic treatment. Teeth were excluded if they exhibited dental caries, visible cracks or fractures, restorations, endodontic therapy, hypoplasia, fluorosis, discoloration, or any developmental or structural anomalies that could affect enamel integrity.[24]

The extracted teeth were stored in a 0.1% thymol solution at 4 °C (BTC, Biotech Company, Cairo, Egypt) to prevent bacterial growth until they were needed again. Before the experiments, they were cleaned with an ultrasonic scaler and thoroughly rinsed with deionized water. This cleaning technique removes dirt and other particles, ensuring that the enamel surface remains undamaged for future examinations.[25] At CEJ, the teeth were coated before being sectioned into slices. The specimens were subsequently embedded in methyl methacrylate resin blocks and affixed to a microtome equipped with a water-cooled diamond blade for longitudinal sectioning. Each crown was sectioned buccally into enamel slabs approximately 2–3 mm thick (Fig. 1). Based on average morphology, each tooth yielded approximately five usable enamel sections per tooth.[26] After sample preparation, the tooth slices from all groups were stored in artificial saliva prepared from analytical-grade reagents for 2 weeks at room temperature, with the solution changed every 3 days.[27]

The specimens of teeth were randomly assigned to five groups using a computer-generated list of random numbers, as detailed below:

- Group I (baseline): sound enamel; no demineralization nor treatment was applied.
- Group II (demineralized): demineralized enamel without further treatment.
- Group III (CS): demineralized enamel treated with CS gel.
- Group IV (Nano-FA): demineralized enamel treated with Nano-FA paste.
- Group V (CS-Nano-FA-CMC): demineralized enamel treated with the combined CS-Nano-FA-CMC paste.

2.4 Enamel demineralization protocol

For Groups II, III, IV, and V, artificial enamel lesions were produced by submerging the crown slabs in a demineralizing solution for 96 h. The solution was refreshed every 24 h to maintain its effectiveness. The demineralization solutions had a pH of 4.2 and consisted of 2.2 M calcium chloride, 2.2 mM sodium phosphate, 0.05 M acetic acid, and 1.0 M potassium hydroxide.[28,29]

2.5 Enamel remineralizing protocol

The laboratory-synthesized materials were applied to the demineralized specimens of the study according to their assigned experimental group, ensuring standardized treatment conditions for the CS, Nano-FA, and the CS-Nano-FA-CMC composite groups. To simulate clinical brushing, each specimen was treated using a soft-tipped microbrush applicator (Microbrush International, USA) to apply the paste with light manual agitation for 1 minute, twice daily, for 14 consecutive days. Approximately pea-sized amounts of paste were applied per specimen. Following each brushing session, the specimens were rinsed with deionized water for 10 seconds and subsequently stored in freshly prepared artificial saliva at 37 °C. Each enamel specimen was evaluated at two stages: after demineralization and following the remineralization period.

2.6 Synthesis of CS hydrogel

The CS hydrogel was synthesized by a documented technique, with modifications implemented to enhance the purity and homogeneity of the final product.[30] A solvent mixture was prepared by combining 300 mL of 10% (w/v) acetic acid with 200 mL of methanol. A 0.1 M NaOH solution was utilized to adjust the pH to 4.0. Once the solution attained stability, 15 g of

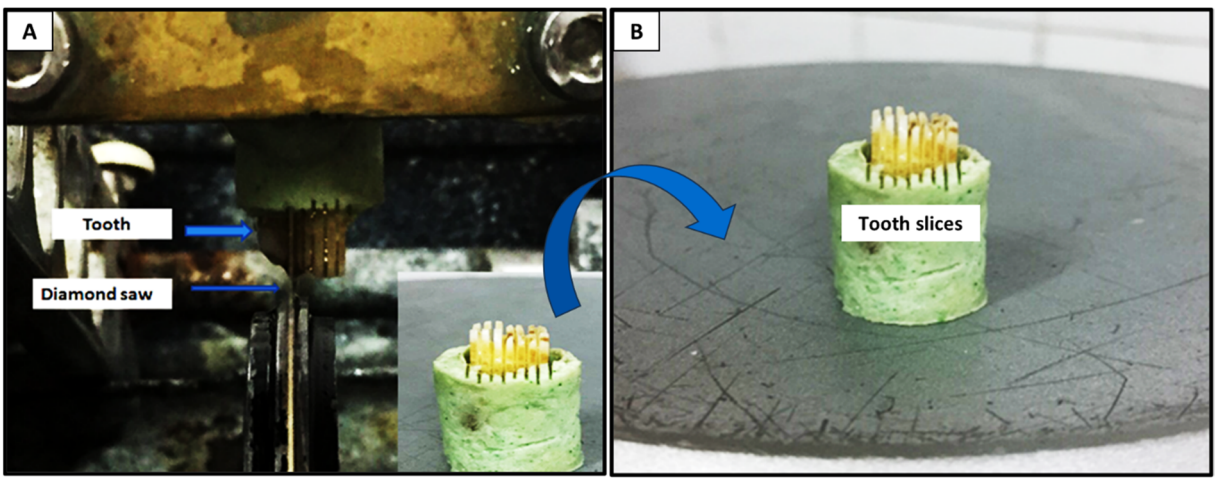

Fig. 1 Tooth sample preparation. (A) A microtome equipped with a water-cooled diamond. (B) The tooth slices.

chitosan powder (yielding a final concentration of 2%) was added at a controlled rate of 0.1 mg every 2 min, while stirring for 2 h. This ensured that the polymer solution was thoroughly and uniformly distributed. Subsequently, while gently stirring, a mixture of 450 mL ethanol and 450 mL ethyl acetate was added incrementally to the chitosan solution. The system was subsequently left undisturbed to facilitate gelation. We purified the residual hydrogel-like material and subsequently washed it for 30 min with a solution containing 210 mL of ethyl acetate and 90 mL of pure ethanol to remove residual solvents. The substance was re-evaluated once it had settled. The semi-solid hydrogel was redissolved in deionized water and carefully transferred to a flask for rotary evaporation. The solvent was extracted at 60 °C under reduced pressure. The concentrated gel was subsequently freeze-dried for 48 hours, yielding a porous chitosan hydrogel powder suitable for further physicochemical analyses.

2.7 Synthesis of Nano-FA powder

We synthesized Nano-FA using a modified sol–gel method designed for biomedical applications, particularly for the remineralization of enamel.[31] Calcium nitrate tetrahydrate ($Ca(NO_3)_2 \cdot 4H_2O$) and phosphorus pentoxide (P_2O_5) were the primary sources of phosphorus and calcium, respectively. Absolute ethanol served as the reaction medium, while hexafluorophosphoric acid (HPF_6) was employed to introduce fluoride ions into the system. In a typical method, 20 mL of 100% ethanol was used to dissolve 7.0 g of $Ca(NO_3)_2 \cdot 4H_2O$, thereby creating a 0.5 M calcium solution. 0.192 g of P_2O_5 was dissolved in 20 mL of ethanol. Then, 1.14 mL of HPF_6 was added slowly while the mixture was stirred with a magnetic stirrer to form a phosphorus-fluoride precursor. The phosphorus fluoride mixture was stirred constantly at room temperature while the calcium solution was slowly added. For 24 h, the mixture was stirred continuously to ensure it became a homogeneous solution. The resulting solution was left to sit for 24 h, allowing it to gel and mature. The gel was then dried at 120 °C for 24 h to remove any remaining solvent. To improve the crystals and eliminate organic by-products, the dried sample was finely ground and then heated to 600 °C for one hour at a rate of 3 °C min^{-1}.

2.8 Synthesis of CS-Nano-FA-CMC nanocomposite hydrogel

We combined the as-synthesized chitosan hydrogel, nano-folic acid powder, and carboxymethyl cellulose in a 1 : 1 : 3 mass ratio while continuously stirring to produce the chitosan-nano-folic acid-carboxymethyl cellulose composite hydrogel.[32] The required amount of Nano-FA powder was gradually added to the chitosan hydrogel solution according to the predetermined mass ratio. Ultrasonic treatment was administered to the mixture for 15 min to enhance the initial dispersion. The mixture was stirred with a magnet at 45 °C for 90 min to facilitate the uniform dispersion of nanoparticles inside the chitosan polymeric matrix. A 2% (w/v) CMC solution was prepared by dissolving the appropriate amount of CMC powder in double-distilled water, then evaporating approximately 75% of the initial volume. After cooling to room temperature, it was slowly introduced to the CS-Nano-FA nanocomposite hydrogel under constant stirring at ambient conditions, forming a uniform white suspension. To induce physical crosslinking, the synthesized CS-Nano-FA-CMC hydrogel was transferred into a scaffold Mold and underwent a freeze–thaw cycle, consisting of freezing at −20 °C for 18 h and thawing at room temperature for 6 h. Upon completion of the cycle, the former scaffold was demoulded and characterized using several techniques to confirm the successful fabrication and structural integrity of the CS-Nano-FA-CMC hydrogel.

2.9 Instrumentation for characterization

A range of analytical techniques was employed to characterize the structural features of the synthesized CS, Nano-FA, and CS-Nano-FA-CMC nanocomposite hydrogel samples. Table 1 summarizes detailed specifications of the instrumentation used.

2.10 Microhardness testing

Ten enamel specimens were subjected to surface microhardness testing in each group using a Vickers microhardness testing equipment (Zwick/Roell, INDENTEC, ZHVμ-S, West Midlands, Angleterre). During the three phases of the study, before, after demineralization, and after remineralization, the specimens' microhardness was assessed. Each specimen had three indentations spaced 100 microns apart, and a 300 g force was applied during a 20 seconds dwell duration. For each sample, the mean hardness value was computed by averaging the values obtained from all three indentations.

2.11 Scanning electron microscopic examination (SEM) and energy dispersive X-ray (EDX) of the specimens

Testing was done at every stage of the investigation. The amounts of calcium and phosphate in the surface enamel of 10 specimens from each group were quantitatively assessed. An SEM equipped with EDX was employed for testing. To evaluate enamel structure, the remaining twenty specimens in each group were seen under a SEM microscope (JEOL JSM-5300-JSM, Tokyo, Japan). For 24–48 h at 4 °C, the samples were fixed in a solution containing 2.5% glutaraldehyde and 2% paraformaldehyde in 0.1 M phosphate buffer (pH 7.2–7.4). Following a distilled water rinse, the teeth were left to soak for an hour at room temperature in a 0.5% sodium hypochlorite (NaOCl) solution. They were then post-fixed in 1% osmium tetroxide for 2 h at 4 °C after being washed with distilled water for 12 h. The specimens were then dried in a critical point drier using liquid CO_2 after being dehydrated using an ascending series of graded ethanol. They were put on metal stubs that had been ion-sputter-coated with gold and palladium.

2.12 Statistical analysis

CO-STAT software (version 6.4) was used to collect, tabulate, and analyze quantitative data from Vickers microhardness and EDX measurements. Descriptive statistics, such as mean,

Table 1 Instruments used and their specifications

Instrument name	Model	Data	Conditions
Fourier-transform infrared spectrophotometer (FT-IR)	A BRUKER VERTEX 70	FT-IR spectrum	400–4000 cm^{-1}
X-ray diffraction (XRD)	Shimadzu LabX 6100, Kyoto, Japan	XRD spectrum	The XRD generator works at 40 kV, 30 mA, $\lambda = 1$ Å, using target Cu Kα with secondary monochromatic X-ray, 2θ from 10° to 80°, recording steps of the diffraction data of 0.02°, at a time of 0.6 s, at room temperature (25 °C)
Scanning electron microscope (SEM)	JSM-lT200, JEOL ltd sputtering coating (JEOL-JFC-1100E)	SEM images	Imaging mode
High-resolution transmission electron microscope (HR-TEM)	JEOL-JSM-1400 plus	TEM image	Imaging mode
Energy dispersive X-ray (EDX)	JSM-lT200, JEOL ltd	EDX spectrum	Acceleration voltage 20.00 kV, WD 10.00 mm, live time 30.00, high vacuum mode

standard deviation, and range, were employed to illustrate numerical variables. *Post hoc* (Tukey) and one-way ANOVA tests were used to compare quantitative data across groups.

3 Results

3.1 Characterization of the CS-Nano-FA-CMC nanocomposite hydrogel

3.1.1 X-ray diffraction (XRD). We employed X-ray diffraction (XRD) analysis to examine the structural characteristics of Nao-FA, CS hydrogel, and the synthesized CS-Nano-FA-CMC nanocomposite hydrogel. The resulting patterns are illustrated in Fig. 2. The XRD pattern depicted in Fig. 2a corresponds to the synthesized Nano-FA. The diffraction profile shows a series of sharp peaks, indicating that the material is highly crystalline. These peaks are characteristic of the FA phase and confirm the successful formation of nanocrystalline $Ca_5(PO_4)_3F$. The results, when compared with the conventional reference pattern (JCPDS card no. 15-0876), demonstrate a high degree of similarity, indicating that the synthesized material possesses a hexagonal crystal structure.[33] The diffractogram shows no additional reflections, indicating the absence of secondary phases or structural imperfections. This provides additional evidence of the product's outstanding purity.

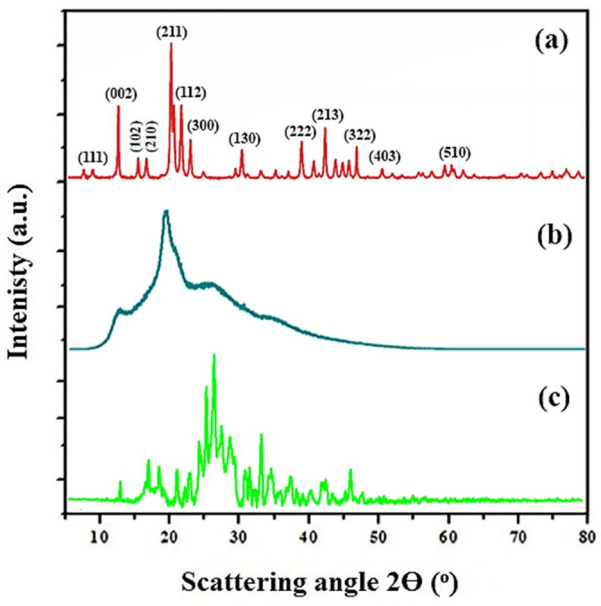

Fig. 2 XRD patterns of (a) Nano-FA, (b) CS hydrogel, and (c) the CS-Nano-FA-CMC nanocomposite hydrogel.

The XRD pattern of the freeze-dried CS hydrogel (Fig. 2b) indicates that it possesses a semi-crystalline structure. A broad peak is evident at 2θ = 22.48°, with minor reflections at approximately $2\theta = 10.32°$ and 26.71°.[34] The diffraction patterns indicate the presence of both ordered and disordered molecular structures within the hydrogel matrix. The peak around 22° is often associated with the reorganization of polymer chains during freeze-drying, indicating that chitosan undergoes partial crystallization. The significant widening of the diffraction peaks, particularly at lower angles, indicates an increased presence of amorphous domains inside the hydrogel matrix. These amorphous regions enhance the hydrogel's water-absorption capacity, thereby increasing its flexibility and growth potential.[35]

The XRD patterns of individual Nano-FA (Fig. 2a) and CS hydrogel (Fig. 2b) functioned as references to facilitate the analysis of the diffractogram for the CS-Nano-FA-CMC nanocomposite hydrogel (Fig. 2c). The nanocomposite pattern showed significant peak broadening, indicating an increase in amorphous material and a decrease in crystalline material compared with the pure CS profile (Fig. 2b). This alteration is substantiated by the disappearance of the CS-specific peak at 2θ = 10.32° and the significant reduction in intensity of the peaks at 22.31° and 26.71°. The reduction in crystalline order can be attributed to robust interactions between CS and CMC molecules and to their adequate mixing within the hydrogel matrix. These interactions likely disrupted the typical arrangement of the polymer chains, complicating the rearrangement of CMC molecules and leading to a more disordered structure.[36] The

slight shift in the positions of the chitosan-related peaks in Fig. 2c suggests that CMC and CS may be capable of cross-linking with one another.[36] Moreover, the characteristic sharp diffraction peaks of Nano-FA, corresponding to the hexagonal fluorapatite phase (JCPDS no. 15-0876), are clearly retained in the composite pattern, confirming the successful incorporation of the inorganic phase without phase transformation. However, the inclusion of Nano-FA did not significantly impact the overall crystallinity of the nanocomposite.[37]

The structural data collectively confirm the successful synthesis of the CS-Nano-FA-CMC nanocomposite under the specified conditions.

3.1.2 FT-IR spectroscopy. FT-IR analysis was employed as the principal analytical technique to confirm the successful integration of components within the synthesized nanocomposite hydrogel, hence demonstrating the effectiveness of the production process. Fig. 3 illustrates the FT-IR spectrum of Nano-FA, CS, and the CS-Nano-FA-CMC nanocomposite hydrogel. This provides insight into the functional groups constituting the composite matrix and their interactions. Fig. 3a illustrates the FT-IR spectra of the synthesized Nano-FA. It exhibits multiple distinct absorption peaks. An inconspicuous absorption band at 3649 cm^{-1} is indicative of the stretching vibration of the OH–F bond. This suggests that fluoride ions may potentially replace hydroxyl groups within the apatite lattice.[33] In the 1400–900 cm^{-1} region, multiple absorption bands corresponding to phosphate (PO_4^{3-}) stretching vibrations are evident, confirming the crystalline nature of the apatite phase.[38] At 1031 cm^{-1}, a distinct band is visible. This is because of the asymmetric stretching mode of PO_4^{3-}. The v_1 band corresponds to the strong bands at 1124 and 964 cm^{-1}, and v_2 corresponds to the symmetric stretching vibrations of phosphate groups.[38]

Fig. 3b presents the FT-IR study of chitosan, revealing multiple distinct vibrational bands associated with its functional groups. An extensive absorption band at 3483 cm^{-1} signifies the stretching vibrations of hydroxyl (–OH) and amine (N–H) groups, along with the effects of intermolecular hydrogen bonding interactions.[39] The peak at 1412 cm^{-1} corresponds to the symmetric bending of methyl groups ($-CH_3$), whilst the shoulder at 1345 cm^{-1} is attributed to the stretching vibration of carboxylate functionalities (O=C–O).[39] Also, faint bands at 1223 cm^{-1} and 1023 cm^{-1} show the asymmetric stretching of ether linkages (C–O–C) and C–O deformations, which confirms that CS has a polysaccharide backbone.[35] The bands at 1644 and 1559 cm^{-1} show the vibrational modes of amide I (C=O stretching) and amide II (N–H bending), respectively. This means that the chitosan structure has lost a significant amount of acetylation.[40] The 1559 cm^{-1} peak may also indicate the formation of imine (C=N) bonds, which would support the formation of Schiff bases and confirm that the hydrogel network is crosslinked.[34] There are further peculiarities in the spectrum, such as a band at 923 cm^{-1}. This band is caused by the overlapping of C–N stretching from primary amines and C–O stretching from primary alcohol groups, which are part of the chitosan structure.[41] A low-intensity band at 680 cm^{-1} is also seen. This band is linked to the angular deformation of H–N–H bending vibrations, which further proves that primary amine functionalities are present.[35]

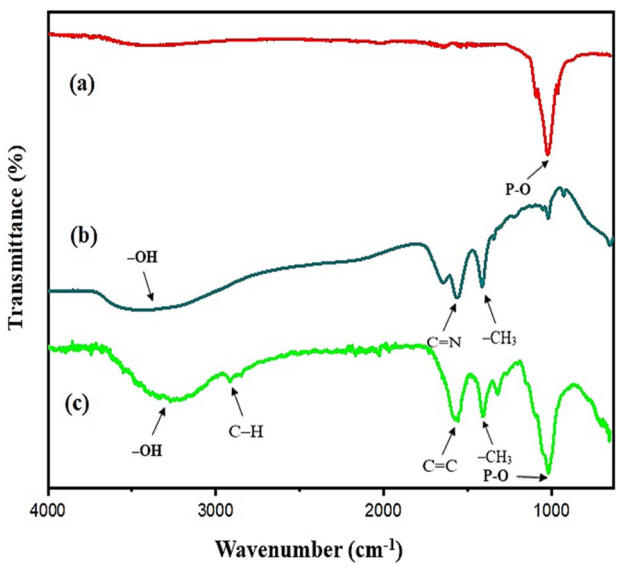

Fig. 3 FT-IR spectra of (a) Nano-FA, (b) CS hydrogel, and (c) the CS-Nano-FA-CMC nanocomposite hydrogel.

Fig. 3c shows the FT-IR spectra of the CS-Nano-FA-CMC nanocomposite. It exhibits multiple strong absorption bands that correspond to the functional groups of its components. The CS-Nano-FA-CMC spectrum shows new characteristic peaks that line up with those of Nano-FA, as well as features that are unique to CMC. This is different from the spectrum of chitosan hydrogel (Fig. 3b). These spectral alterations, such as small wavenumber shifts and intensity changes, indicate molecular-level interactions between the components of the hybrid system. The absorption bands at 1058 and 2030 cm^{-1} are important because they are associated with C–O and C–H stretching vibrations, respectively. The peaks at 2327, 2134, and 1946 cm^{-1} also indicate C=O stretching in the six-membered ring structure of CMC, confirming its successful incorporation into the nanocomposite network.[42] The absorption bands at 3483, 1644, and 1559 cm^{-1} also indicate that the typical vibrational modes of CMC and CS overlap, suggesting that they have been well integrated into the nanocomposite matrix. The considerable shift of these bands towards lower wavenumbers suggests that the stretching motions of free O–H and N–H groups are limited. This is often thought to result from stronger intermolecular hydrogen bonds forming between chitosan, Nano-FA, and CMC chains. This redshift phenomenon corroborates chemical interactions that reinforce the hydrogel network. Shahzad *et al.* also saw a similar change in the O–H stretching area in their study on carboxymethyl/chitosan/gelatin/PEG-GO nanocomposite hydrogels, which supports this proposal.[41]

3.1.3 Energy dispersive X-rays (EDX). Using EDX analysis, we systematically examined the chemical composition and elemental profile of Nano-FA, CS, and the resulting CS-Nano-FA-CMC nanocomposite hydrogel, as illustrated in Fig. 4. The EDX spectrum of Nano-FA (Fig. 4a) showed clear signals for oxygen (40.16%), fluorine (9.56%), phosphorus (13.65%), and calcium

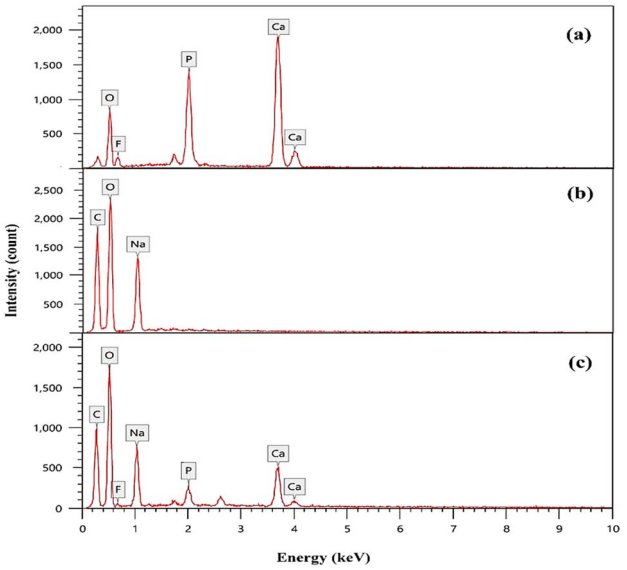

Fig. 4 EDX spectra of (a) Nano-FA, (b) CS, and (c) the CS-Nano-FA-CMC nanocomposite hydrogel.

(30.04%). There were also small amounts of carbon and silicon, which were likely remnants of impurities. These data demonstrate that Nano-FA powder was successfully produced. The elemental analysis showed that the Ca/P molar ratio was about 1.70, which is higher than the expected stoichiometric ratio of 1.67 for perfect fluorapatite ($Ca_{10}(PO_4)_6F_2$). This slight rise in the Ca/P ratio could mean that calcium is somewhat more abundant or that the apatite lattice has modest structural changes. These phenomena have been correlated with increased material stability and bioactivity.[43]

The EDX spectrum of the chitosan hydrogel (Fig. 4b) also shows clear peaks for carbon (39.41%) and oxygen (48.14%), as well as a small amount of salt. The strong signals from carbon and oxygen are consistent with chitosan's organic, polysaccharide structure and numerous hydroxyl and amino functional groups. Sodium at low concentrations may be present as a byproduct of chemicals used in synthesis or purification. The absence of other elements further supports the high purity of the chitosan hydrogel matrix used in the nanocomposite formation.

The EDX analysis of the CS-Nano-FA-CMC nanocomposite hydrogel (Fig. 4c) showed that it was mostly made up of carbon (31.56%) and oxygen (47.63%). This is because CS and CMC produced an organic polymeric network. Additionally, the presence of fluorine (2.28%), phosphorus (1.50%), and calcium (6.45%) substantiates the successful integration and uniform distribution of Nano-FA inside the hydrogel matrix. This well-integrated organic–inorganic interface is crucial for enhancing the hydrogel's effectiveness in dental demineralization.

3.2 SEM and TEM microstructural analysis

A comprehensive assessment of the morphological characteristics and internal microstructure of hydrogels is crucial for comprehending their functional behavior, especially in biomedical contexts. This study investigated the structural characteristics of the freeze-dried CS-Nano-FA-CMC nanocomposite hydrogel and Nano-FA using scanning electron microscopy (SEM) and transmission electron microscopy (TEM). These methods give us important information about the hydrogel's surface topology and porosity structure. A porous, connected network makes the hydrogel better at supporting tooth remineralization. Fig. 5a shows the SEM image of Nano-FA. In contrast, Fig. 5b illustrates the TEM morphology of Nano-FA, and Fig. 5c presents the SEM microstructure of the CS-Nano-FA-CMC composite hydrogel, highlighting the formation of an interconnected network after polymer incorporation. The SEM image of the Nano-FA particles (Fig. 5a) shows well-defined hexagonal shapes with an average diameter of approximately 47.68 nm. The TEM study (Fig. 5b) corroborates these structural characteristics, displaying elongated, needle-like particle arrangements with slight size variations, consistent with the SEM findings. The Nano-FA particles exhibited a uniform spatial distribution and minimal agglomeration, indicating that the synthesis process effectively controlled particle shape. This kind of nanoscale homogeneity and dispersion is crucial for ensuring that the materials mix well with composite hydrogel matrices and that ions are released consistently, especially when the goal is to remineralize enamel.

The SEM micrograph of the CS-Nano-FA-CMC nanocomposite hydrogel (Fig. 5c) exhibits a three-dimensional structure that is very porous and has many connections, which is typical of hydrogel matrices made from CS.[44] The structure has long tubular shapes with microchannels that are not evenly spaced. This indicates that the pore system is open and varied, allowing for controlled diffusion and sustained release of Ca^{2+}, PO_4^{3-}, and F^- ions. These ions are necessary for apatite nucleation and the growth of enamel crystals. Additionally, Nano-FA appears as separate, brilliant particles evenly distributed throughout the chitosan framework, with only small areas of aggregation. The uniform distribution is probably due to intermolecular hydrogen bonding between Nano-FA and the surrounding CS-CMC matrix. This makes the interface stronger and helps the structure come together. The SEM image reveals no signs of phase separation or isolated domains, indicating that the composite components are highly compatible and homogeneous at the molecular level. The bioactive, high-surface-area scaffold ensures strong adhesion to demineralized enamel surfaces.

3.3 Scanning electron microscopic results

Group I (baseline): showed a typical sound enamel surface with smooth architecture and a prismatic enamel covering the outer enamel surface (Fig. 6A).

Group II (demineralized) showed demineralized enamel with uneven depressions distributed nearly all over the surface (Fig. 6B).

Group III (CS) exhibited enamel with large calcium crystals distributed uniformly across the surface, accompanied by small depressions between the crystals (Fig. 6C).

Group IV (Nano-FA) showed enamel with large calcium crystals distributed over the surface. These crystals coalesced, forming large, mineralized masses with small depressions between them (Fig. 6D).

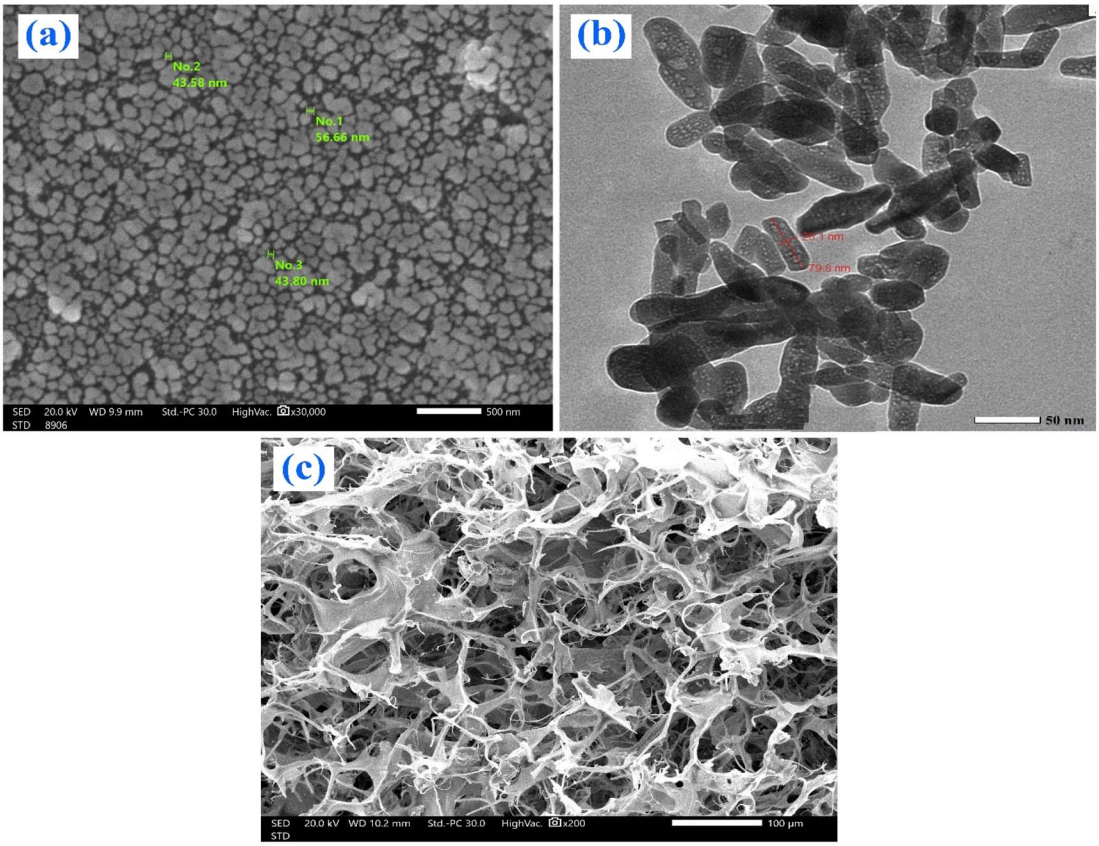

Fig. 5 Microstructural characterization of the synthesized materials: (a) SEM image of Nano-FA showing well-defined hexagonal nanoparticles, (b) TEM image of Nano-FA illustrating elongated needle-like morphology, (c) SEM image of the CS-Nano-FA-CMC nanocomposite hydrogel showing a three-dimensional porous network with uniformly distributed nanoparticles.

Group V (CS-Nano-FA-CMC) showed enamel surface remineralization, forming large, smooth areas that appear wide and cover nearly the whole enamel surface, except at small and tiny depressions (Fig. 6E and F).

3.4 Statistical analysis of Vickers hardness test

Table 2 and Fig. 7 display the mean and standard deviation (SD) of Vickers Hardness Number (VHN) for all specimens. A considerable improvement in the surface VHN was observed in the treated specimens compared to their associated demineralized values. According to the Tukey multiple-comparison test, surface microhardness increased significantly in Group III ($p < 0.05$). At the same time, Groups IV and V exhibited a highly significant increase ($p < 0.001$) when compared to Group II. Interestingly, Groups IV and V showed an enhancement in the mean VHN of enamel, bringing it closer to the baseline values. This indicates a significant increase in surface hardness with both Nano-FA and CS-Nano-FA-CMC.

3.5 Statistical analysis of the (Ca/P) content and (Ca/P) ratio obtained by EDX analysis

The weight percentages of Ca and P in the specimens were analyzed. The Ca and P concentrations were subsequently converted to Ca/P ratios for each group, as shown in Table 3 and Fig. 8. Following demineralization, Group II exhibited a significantly lower Ca/P ratio than Group I's baseline value. Additionally, Groups III and IV exhibited a significant increase in the Ca/P ratio following treatment ($p < 0.05$) compared with Group I, and their results showed no significant difference from baseline enamel Ca/P ratios. Furthermore, Group V demonstrated a significantly larger difference in the mean Ca/P ratio ($p < 0.001$) compared to the other test groups after remineralization, with values that were notably higher than baseline measurements.

4 Discussion

Enamel demineralization poses a significant challenge to oral health, occurring when the balance between demineralization and remineralization is disrupted.[45] Enamel does not regenerate; thus, it cannot repair itself naturally after damage occurs, as ameloblasts are lost following tooth eruption. Demineralization treatment employs non-invasive techniques to accelerate remineralization and inhibit lesion progression. CS has shown considerable promise in enamel remineralization due to its positively charged amino groups, which facilitate electrostatic interactions with the negatively charged enamel surface and bacterial cell walls. This prevents biofilm formation and facilitates the transport of calcium and phosphate ions to

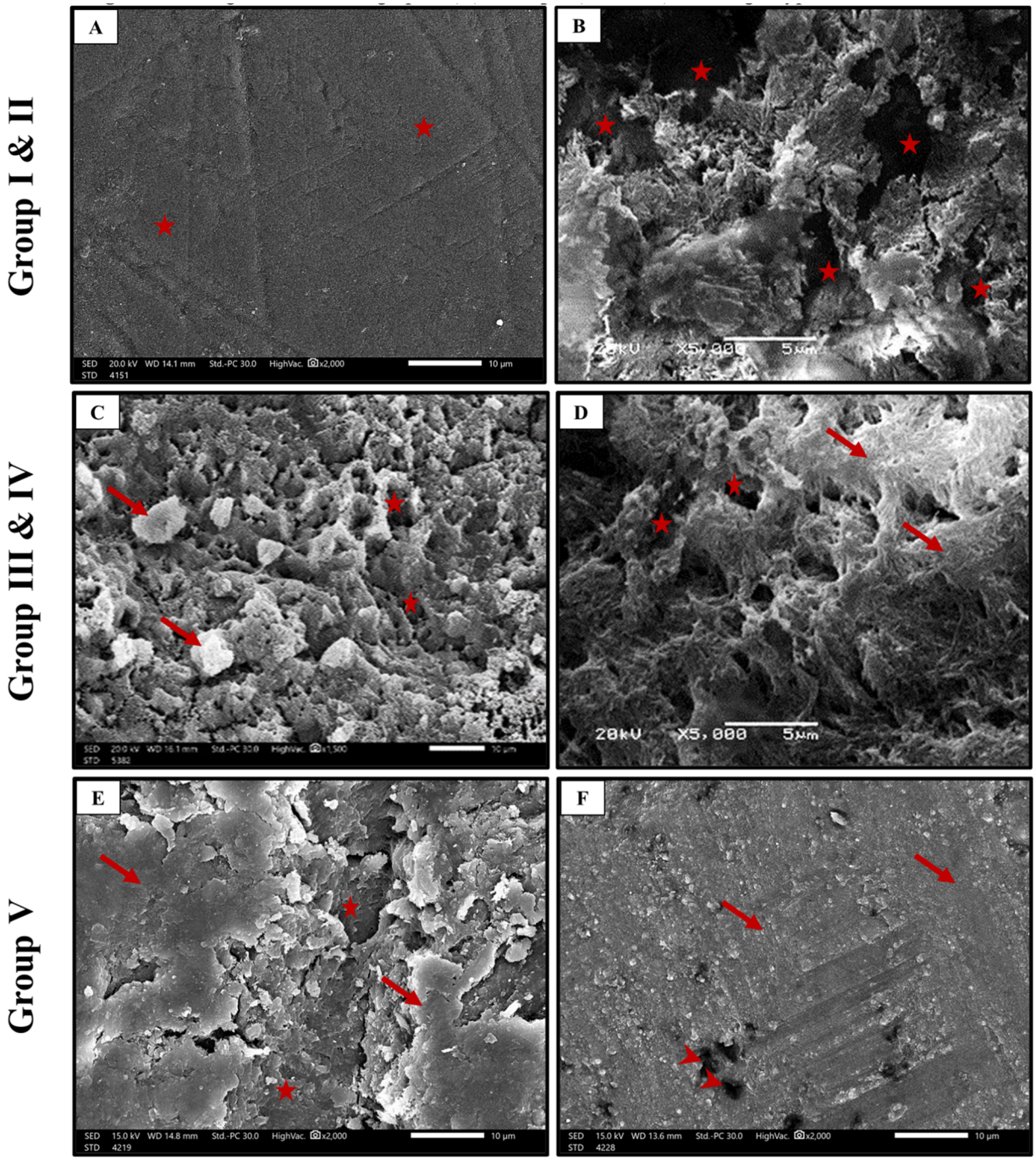

Fig. 6 Scanning electron micrographs: (A) Group I (baseline) showing a typical sound enamel surface with smooth enamel architecture and a prismatic enamel (stars) covering the outer enamel surface. (B) Group II (demineralized) exhibits demineralized enamel with uneven depressions (stars) distributed nearly uniformly over the surface. (C) Group III (CS) exhibits enamel covered with numerous large calcium crystals (arrows) distributed uniformly across the surface, with small depressions (stars) present between the crystals. (D) Group IV (Nano-FA) exhibits enamel covered with numerous large calcium crystals distributed uniformly across the surface, which have coalesced with each other to form large, mineralized masses (arrows) with small depressions (stars) between the crystals. (E and F) Group V (CS-Nano-FA-CMC) shows enamel surface mineralization forming large smooth areas (arrows) which appear wide at E and cover nearly the whole enamel surface at F, except at small depressions (stars) and tiny depressions (arrowheads). SEM, original magnification; (A, C, E & F × 2000, B & D × 5000).

mineral-deficient areas.[12] However, studies indicate that CS-based remineralization systems exhibit limitations, including lower remineralization efficacy than fluoride and inferior mechanical properties.[46] Furthermore, innovative biomimetic strategies employing Nano-HA or Nano-FA, peptide-based scaffolds, and ion-releasing restorative materials have demonstrated potential in improving the natural repair mechanisms of initial lesions.[47,48] Nonetheless, these approaches often exhibit

Table 2 Comparison between the studied groups regarding VHN[a]

Group	Min	Max	Mean ± SD
Baseline	250	399	319.21 ± 44.88
Demineralized enamel	150	190	161.72 ± 11.81
Nano-FA	210	295	270.77 ± 24.27
CS	100	208	180.85 ± 31.12
CS-Nano-FA-CMC	235	280	258.97 ± 14.70

[a] ANOVA: $F = 213.4$, $P = 0.0001$ ($P < 0.05$ considered significant).

Table 3 Comparison between the studied groups regarding elemental composition obtained from EDX analysis (atomic %)[a]

Group	Min	Max	Mean ± SD
Baseline	94.9	99.5	96.96 ± 1.49
Demineralized enamel	43.2	45.6	44.27 ± 0.73
Nano-FA	70.4	73.5	71.96 ± 0.88
CS	69.56	71.42	70.59 ± 0.57
CS-Nano-FA-CMC	88.5	95.3	92.20 ± 2.17

[a] ANOVA: $F = 158.5$, $P = 0.001$ ($P < 0.05$ considered significant).

limited penetration into enamel subsurface lesions and tend to favor surface remineralization.[49] Thus, in this study, we evaluated the effectiveness of combining CS and Nano-FA with CMC paste for enamel remineralization.

The results of the present study confirm the effectiveness of the CS-Nano-FA-CMC nanocomposite in enhancing enamel remineralization, as demonstrated by SEM, EDX, and microhardness analyses. SEM revealed improved surface morphology with mineral deposition, while EDX showed an increase in Ca/P ratio, indicating enhanced mineral content. This was further supported by the recovery in microhardness values, reflecting an improvement in enamel function. From a chemical perspective, the remineralization mechanism of the CS-Nano-FA-CMC system is driven by synergistic interactions among its components. Chitosan, with its positively charged amino groups ($-NH_3^+$), electrostatically interacts with the negatively charged demineralized enamel surface, facilitating adhesion and acting as a nucleation template. Simultaneously, Nano-FA provides a direct source of Ca^{2+}, PO_4^{3-}, and F^- ions, which contribute to the formation of fluorapatite crystals. The presence of CMC enhances system stability by forming a hydrated polymeric network that controls ion diffusion and prolongs ion release. This environment promotes supersaturation of calcium and phosphate ions at the enamel interface, leading to nucleation and growth of apatite crystals within enamel microporosities. Furthermore, the formation of fluorapatite ($Ca_5(PO_4)_3F$) is thermodynamically favored under these conditions, thereby improving acid resistance and structural stability compared to hydroxyapatite. Collectively, these interactions highlight the role of the organic–inorganic hybrid system in achieving effective and sustained enamel remineralization.

In addition to the morphological and compositional findings, the system's physicochemical characteristics further support its performance. FT-IR results confirmed the presence of functional groups capable of forming hydrogen-bonding interactions between CS, CMC, and Nano-FA, contributing to the stability of the composite network. XRD analysis revealed a reduction in crystallinity and an increase in amorphous regions within the composite, facilitating ion diffusion and

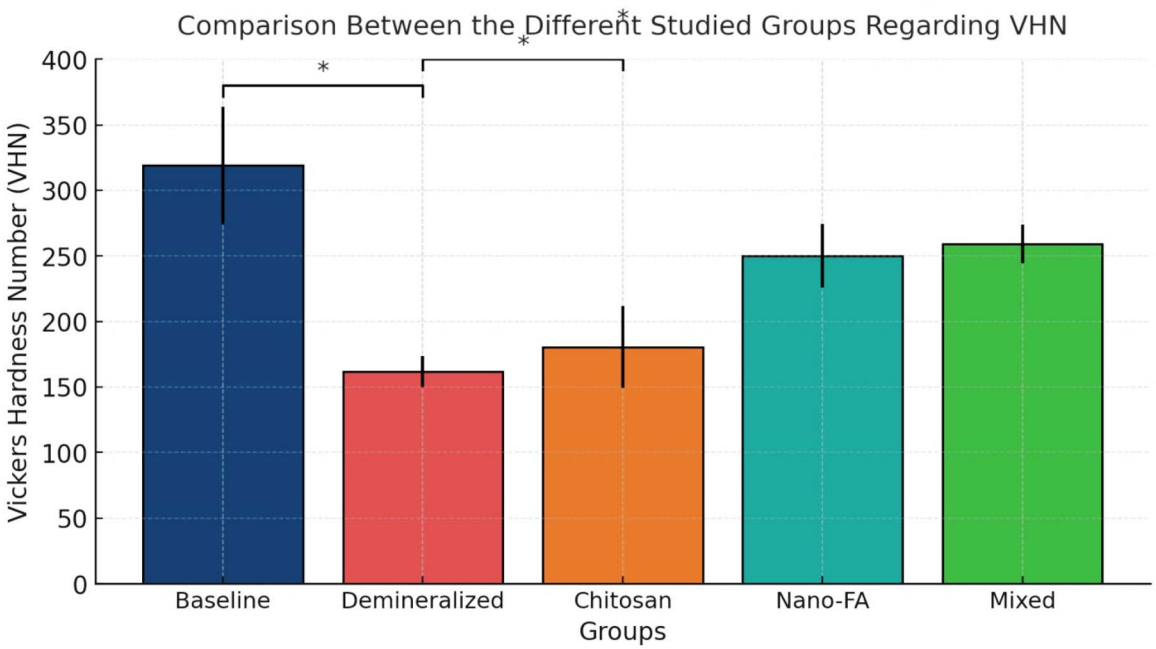

Fig. 7 Box plot to compare the different studied groups regarding VHN.

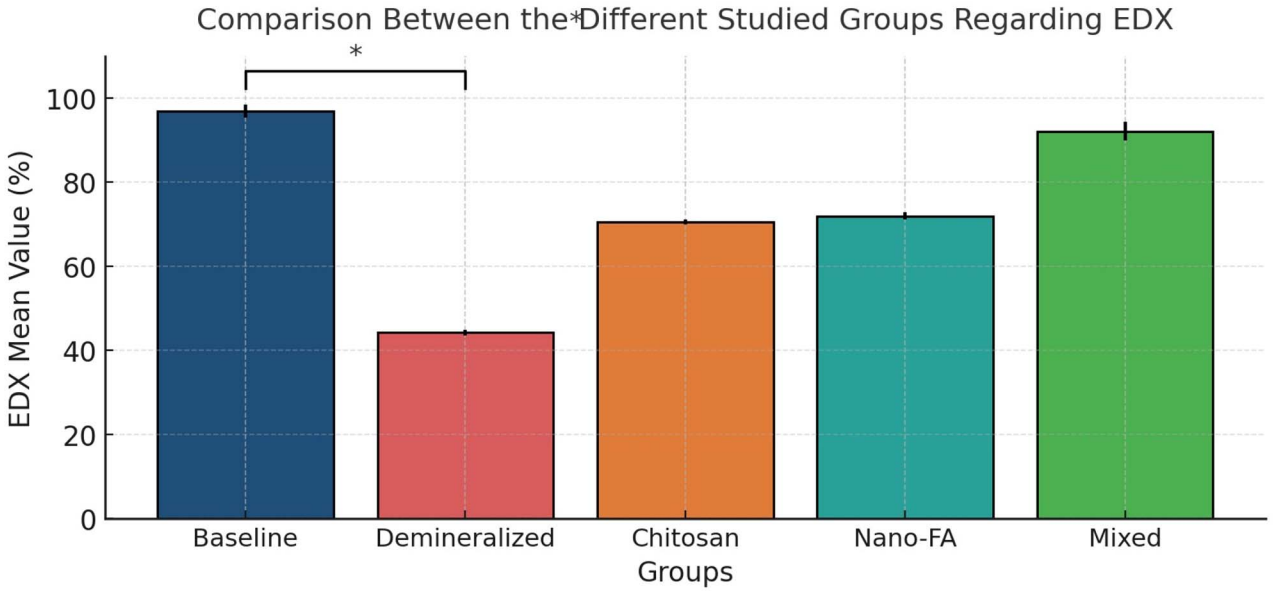

Fig. 8 Box plot to compare the different studied groups regarding EDX.

enhancing the release of Ca^{2+}, PO_4^{3-}, and F^- ions. The semi-crystalline nature of chitosan supports both ion mobility through amorphous regions and structural reinforcement through crystalline domains, confirming its suitability as a delivery matrix for remineralization.[50]

The findings of the present study are consistent with previous reports demonstrating the remineralization potential of chitosan-based systems and nano-calcium phosphate materials. Several studies have shown that chitosan enhances mineral deposition due to its bioadhesive and ion-binding properties,[11,12] while nano-hydroxyapatite and fluorapatite improve enamel microhardness and mineral content.[13,15,48] However, unlike earlier studies that investigated these materials individually, the present work demonstrates a synergistic effect achieved through their combination within a CMC-based matrix. This integrated system enhances ion availability while improving their retention and controlled release at the enamel surface. Consequently, the CS-Nano-FA-CMC system exhibited superior remineralization outcomes compared to previously reported single-component systems.

The synthesis of Nano-FA powder yielded nanosized particles with high phase purity and an appropriate Ca/P molar ratio (~1.67), making them suitable for dental applications aimed at restoring enamel mineral content and structural integrity. Conventional fluoride in toothpaste functions by interacting with calcium and phosphate from saliva to form fluorapatite on the tooth surface. In contrast, Nano-FA inherently contains calcium, phosphate, and fluoride within its crystalline structure, enabling direct deposition onto demineralized enamel. Due to its nanoscale size, it can effectively adhere to enamel and occupy microporosities.[32]

The amorphous and crystalline phases of chitosan play complementary roles in biomimetic remineralization. The amorphous phase facilitates ion diffusion and initiates crystal formation, while the crystalline phase provides mechanical strength and supports progressive mineralization. When combined with CMC, a flexible, hydrated polymeric network forms, enhancing ion transport and prolonging ion availability at the enamel interface. This improves penetration into enamel microporosities compared to Nano-FA alone, which tends to accumulate on the surface and form a barrier that may limit deeper ion diffusion. These synergistic properties support the CS-Nano-FA-CMC hydrogel's dual role as both a scaffold and a nucleation platform for apatite formation.

The biomimetic behavior of the system is further supported by the similarity between chitosan and amelogenin, the natural protein that guides enamel crystal growth. The positively charged amino groups of chitosan promote ordered crystal orientation, while Nano-FA provides a pre-formed crystalline framework that facilitates apatite nucleation and growth. Additionally, hydrogen-bonding interactions within the composite enhance structural stability and regulate ion release, further contributing to effective remineralization.

It is important to note that the evaluation methods employed in the present study, including SEM, EDX, and surface microhardness testing, are predominantly surface-sensitive techniques. Therefore, the observed improvements mainly reflect surface remineralization rather than providing conclusive evidence of subsurface lesion recovery. This limitation is particularly relevant for nano-calcium phosphate systems, where mineral deposition tends to occur preferentially at the outer enamel surface, potentially restricting deeper ion penetration. However, the hydrated polymeric network of the CS-Nano-FA-CMC system may enhance sustained ion release and diffusion into enamel microporosities over time. Nevertheless, this effect cannot be definitively confirmed within the current study. Accordingly, further investigations using depth-resolved techniques such as transverse microradiography (TMR), cross-

sectional microhardness profiling, or micro-computed tomography (micro-CT) are required to accurately evaluate the extent and depth of remineralization.

5 Conclusion

The present study demonstrated that although CS and Nano-FA individually exhibit favorable remineralization potential, the novel CS-Nano-FA-CMC nanocomposite paste showed enhanced enamel remineralization, which may be attributed to synergistic interactions among its components and to the potential role of CMC as a stabilizing polymeric matrix.

Author contributions

Rehab M. El-Sharkawy: methodology, conceptualization, data curation, investigation, visualization, formal analysis, writing – original draft, writing – review & editing. Rania A. Hanafy: methodology, conceptualization, data curation, investigation, formal analysis, visualization, writing – original draft, writing – review & editing. Wafaa Yahia Alghonemy: methodology, conceptualization, data curation, investigation, visualization, formal analysis, writing – original draft, writing – review & editing. Omnia M. Abdelfatah: data curation, methodology. Eman M. Salem: methodology, conceptualization, data curation, investigation, visualization, formal analysis, writing – review & editing. All the authors reviewed the results and approved the final version of the manuscript.

Conflicts of interest

The authors declare no conflicts of interest relevant to this article.

Data availability

On reasonable request, the datasets used and analyzed in the present study are available from the corresponding author.

References

1 M. Barani-Sveçla and S. Buleshkaj, Etiopathogenesis of dental caries, in *Enamel and Dentin-Pulp Complex*. IntechOpen, 2024.
2 N. B. Pitts, D. T. Zero, P. D. Marsh, K. Ekstrand, J. A. Weintraub, F. Ramos-Gomez, *et al.*, Dental caries, *Nat. Rev. Dis. Primers*, 2017, **3**, 1–16.
3 I. Farooq and A. Bugshan, The role of salivary contents and modern technologies in the remineralization of dental enamel: a narrative review, *F1000Res.*, 2021, **9**, 171.
4 G. Malcangi, A. Patano, R. Morolla, M. De Santis, F. Piras, V. Settanni, *et al.*, Analysis of dental enamel remineralization: a systematic review of technique comparisons, *Bioengineering*, 2023, **10**, 472.
5 K. Manjunath and B. Sivapathasundharam, Analysis of enamel rod end pattern at different levels of enamel and its significance in ameloglyphics, *J. Forensic Res.*, 2014, **5**, 1.
6 F. Bröseler, C. Tietmann, C. Bommer, T. Drechsel, M. Heinzel-Gutenbrunner and S. Jepsen, Randomized clinical trial investigating self-assembling peptide P11-4 in the treatment of early caries, *Clin. Oral Invest.*, 2020, **24**, 123–132.
7 M. Reguzzoni, A. Carganico, D. Lo Presti, P. A. Zecca, E. I. Scurati, M. Caccia, *et al.*, Assessment of the Effects of Enamel Remineralization After Treatment with Hydroxylapatite Active Substance: SEM Study, *Appl. Sci.*, 2024, **15**, 3.
8 H. M. Elgamily, E. M. Safwat and A. M. Youssef, Development of a novel Agarose/Nano-Hydroxyapatite/Grape seed extract hydrogel for biomimetic remineralization of demineralized human enamel (An In-Vitro Study), *Sci. Rep.*, 2025, **15**, 26086.
9 E. A. Elshenawy, S. B. Alawy, W. Y. Alghonemy and A. I. El Dosoky, Preventing white spot lesions around orthodontic brackets: efficacy of pre-reacted glass-ionomer barrier coat *versus* silver diamine fluoride: an *in vitro* study, *BDJ Open*, 2025, **11**, 45.
10 H.-P. Yu and Y.-J. Zhu, Guidelines derived from biomineralized tissues for design and construction of high-performance biomimetic materials: from weak to strong, *Chem. Soc. Rev.*, 2024, **53**, 4490–4606.
11 Q. Ruan, D. Liberman, R. Bapat, K. B. Chandrababu, J.-H. Phark and J. Moradian-Oldak, Efficacy of amelogenin-chitosan hydrogel in biomimetic repair of human enamel in pH-cycling systems, *J. Biomed. Eng. Inform.*, 2016, **2**, 119.
12 V. Muşat, E. M. Anghel, A. Zaharia, I. Atkinson, O. C. Mocioiu, M. Buşilă, *et al.*, A chitosan–agarose polysaccharide-based hydrogel for biomimetic remineralization of dental enamel, *Biomolecules*, 2021, **11**, 1137.
13 A. Juntavee, N. Juntavee and P. Hirunmoon, Remineralization potential of nanohydroxyapatite toothpaste compared with tricalcium phosphate and fluoride toothpaste on artificial carious lesions, *Int. Dent. J.*, 2021, **2021**, 5588832.
14 E. Paszynska, M. Pawinska, J. Enax, F. Meyer, E. Schulze zur Wiesche, T. W. May, *et al.*, Caries-preventing effect of a hydroxyapatite-toothpaste in adults: an 18-month double-blinded randomized clinical trial, *Front. Public Health*, 2023, **11**, 1199728.
15 Q. Yang, F. Li, Y. Ye and X. Zhang, Antimicrobial, remineralization, and infiltration: advanced strategies for interrupting dental caries, *Med. Rev.*, 2025, **5**, 87–116.
16 J. Liao, J. Qiu, Y. Lin and Z. Li, The application of hydrogels for enamel remineralization, *Heliyon*, 2024, **10**, e33574, DOI: 10.1016/J.HELIYON.2024.E33574.
17 M. S. Rahman, M. S. Hasan, A. S. Nitai, S. Nam, A. K. Karmakar, M. S. Ahsan, *et al.*, Recent developments of carboxymethyl cellulose, *Polymers*, 2021, **13**, 1345.
18 J. Fan, P. Wang, S. Wang, R. Li, Y. Yang, L. Jin, *et al.*, Advances in macro-bioactive materials enhancing dentin bonding, *Discover Nano*, 2025, **20**, 1–24.
19 V. Guarnizo-Herrero, C. Torrado-Salmerón, N. S. Torres Pabon, G. Torrado Durán, J. Morales and S. Torrado-Santiago, Study of different chitosan/sodium

carboxymethyl cellulose proportions in the development of polyelectrolyte complexes for the sustained release of clarithromycin from matrix tablets, *Polymers*, 2021, **13**, 2813.
20 W. M. Association, World Medical Association Declaration of Helsinki: ethical principles for medical research involving human participants, *JAMA*, 2025, **333**, 71–74.
21 J. Charan and T. Biswas, How to calculate sample size for different study designs in medical research?, *Indian J. Psychol. Med.*, 2013, **35**, 121–126.
22 F. Faul, E. Erdfelder, A.-G. Lang and A. Buchner, G* Power 3: A flexible statistical power analysis program for the social, behavioral, and biomedical sciences, *Behav. Res. Methods*, 2007, **39**, 175–191.
23 K. I. Reid, Informed consent in dentistry, *J. Law Med. Ethics*, 2017, **45**, 77–94.
24 J.-H. Kim, S. Kim and Y.-S. Park, Effects of a commercial whitening toothpaste containing hydrogen peroxide and citric acid on dentin abrasion and erosion, *BMC Oral Health*, 2023, **23**, 619.
25 A. R. D. Freitas, F. D. D. C. Aznar, A. L. D. Silva, A. Sales-Peres and S. H. D. C. Sales-Peres, Assessment of the effects of decontamination and storage methods on the structural integrity of human enamel, *Rev. Odontol. UNESP*, 2016, **45**, 59–64.
26 A. Jablonski-Momeni and V. Stachniss, Serial sectioning of teeth and microscopy in cariology research, in *Microscopy: Science, Technology, Applications and Education*, 2010, pp. 785–791.
27 K. Raum, K. Kempf, H. J. Hein, J. Schubert and P. Maurer, Preservation of microelastic properties of dentin and tooth enamel in vitro—A scanning acoustic microscopy study, *Dent. Mater.*, 2007, **23**, 1221–1228, DOI: 10.1016/J.DENTAL.2006.11.009.
28 P. Tschoppe, A. M. Kielbassa and H. Meyer-Lueckel, Evaluation of the remineralising capacities of modified saliva substitutes in vitro, *Arch. Oral Biol.*, 2009, **54**, 810–816.
29 M. B. Helal, M. S. Sheta and W. Y. Alghonemy, Comparing the remineralization potential of undemineralized dentin powder *versus* chicken eggshell powder on artificially induced initial enamel carious lesions: an in-vitro investigation, *BMC Oral Health*, 2024, **24**, 1048.
30 Y. Xu, J. Han and H. Lin, Fabrication and characterization of a self-crosslinking chitosan hydrogel under mild conditions without the use of strong bases, *Carbohydr. Polym.*, 2017, **156**, 372–379.
31 C. Li, G. Wang, S. Wang, W. Shen, Y. Zhang, J. Kang, *et al.*, Fluorapatite Glass-Ceramics in Dentistry: Synthesis, Properties, Forming Technology, Applications, Challenges, and Future Perspectives, *Materials*, 2025, **18**, 804.
32 N. Y. Elmehbad, N. A. Mohamed, N. A. Abd El-Ghany and M. M. Abdel-Aziz, Reinforcement of the antimicrobial activity and biofilm inhibition of novel chitosan-based hydrogels utilizing zinc oxide nanoparticles, *Int. J. Biol. Macromol.*, 2023, **246**, 125582.
33 E. M. Salem, O. M. Abdelfatah, R. A. Hanafy, R. M. El-Sharkawy, G. Elnawawy and W. Y. Alghonemy, Comparative study of pulpal response following direct pulp capping using synthesized fluorapatite and hydroxyapatite nanoparticles, *BMC Oral Health*, 2025, **25**, 17.
34 Z. Chen, Z.-B. Zhang, J. Zeng, Z.-J. Zhang, S. Ma, C.-M. Tang, *et al.*, Preparation of polyethyleneimine-modified chitosan/Ce-UIO-66 composite hydrogel for the adsorption of methyl orange, *Carbohydr. Polym.*, 2023, **299**, 120079.
35 Z. Lu, L. Zou, X. Zhou, D. Huang and Y. Zhang, High strength chitosan hydrogels prepared from NaOH/urea aqueous solutions: the role of thermal gelling, *Carbohydr. Polym.*, 2022, **297**, 120054.
36 V. Pitpisutkul and J. Prachayawarakorn, Hydroxypropyl methylcellulose/carboxymethyl starch/zinc oxide porous nanocomposite films for wound dressing application, *Carbohydr. Polym.*, 2022, **298**, 120082.
37 P. Kanmani and J.-W. Rhim, Properties and characterization of bionanocomposite films prepared with various biopolymers and ZnO nanoparticles, *Carbohydr. Polym.*, 2014, **106**, 190–199.
38 Y. Moayedee, I. Mobasherpour, S. Banijamali, M. Razavi and N. Nezafati, Effect of the nano-fluorapatite ceramic particles on mechanical behavior of fluoride varnishes, *Mater. Chem. Phys.*, 2022, **288**, 126421.
39 L. Zhang, X. Bai, Y. Liang, G. Zhang, J. Zou, W. Lai, *et al.*, Preparation of chitosan derivatives/oxidized carboxymethyl cellulose hydrogels by freeze-thaw method: Synthesis, characterization, and utilization in dye absorption, *Int. J. Biol. Macromol.*, 2024, **282**, 136924.
40 A. Rahmatpour and A. H. A. Hesarsorkh, Chitosan and silica nanoparticles-modified xanthan gum-derived bio-nanocomposite hydrogel film for efficient uptake of methyl orange acidic dye, *Carbohydr. Polym.*, 2024, **328**, 121721.
41 K. Shahzad, M. A. Raza, A. Hussain, K.-C. Ko, H.-J. Jeong, K.-K. Seralathan, *et al.*, Synthesis and characterization of self-crosslinked carboxymethyl chitosan-based hydrogel and its composites with gelatin and PEG-GO for drug delivery applications, *Int. J. Biol. Macromol.*, 2025, **308**, 142256.
42 X. Yu, Y. Yang, Q. Liu, Z. Jin and A. Jiao, A hydroxypropyl methylcellulose/hydroxypropyl starch nanocomposite film reinforced with chitosan nanoparticles encapsulating cinnamon essential oil: Preparation and characterization, *Int. J. Biol. Macromol.*, 2023, **242**, 124605.
43 C. Y. Tan, R. Singh, Y. C. Teh, Y. M. Tan and B. K. Yap, The effects of the calcium-to-phosphorus ratio on the densification and mechanical properties of hydroxyapatite ceramic, *Int. J. Appl. Ceram. Technol.*, 2015, **12**, 223–227.
44 C. Tang, Y. Xu, Y. Xie, X. Liu, Z. Wang, H. Zhou, *et al.*, Mechanisms of gel formation in collagen/hydroxypropyl methylcellulose aqueous mixtures below the threshold for macroscopic phase separation, *Int. J. Biol. Macromol.*, 2025, **308**, 142407.
45 O. Fejerskov, B. Nyvad and E. Kidd, *Dental Caries: the Disease and its Clinical Management*, John Wiley & Sons, 2015.
46 L. Basir, R. Meshki, H. Aghababa and V. Rakhshan, Effects of three commercial toothpastes incorporating "chitosan, casein phosphopeptide-amorphous calcium phosphate, sodium monofluorophosphate, and sodium fluoride" on

remineralization of incipient enamel caries in the primary dentition: A preliminary *in vitro* study, *Dent. Res. J.*, 2020, **17**, 433–438.

47 A. Upadhyay, S. Pillai, P. Khayambashi, H. Sabri, K. T. Lee, M. Tarar, *et al.*, Biomimetic aspects of oral and dentofacial regeneration, *Biomimetics*, 2020, **5**, 51.

48 M. Du, J. Chen, K. Liu, H. Xing and C. Song, Recent advances in biomedical engineering of nano-hydroxyapatite including dentistry, cancer treatment and bone repair, *Composites, Part B*, 2021, **215**, 108790.

49 M. Memarpour, F. Shafiei, A. Rafiee, M. Soltani and M. H. Dashti, Effect of hydroxyapatite nanoparticles on enamel remineralization and estimation of fissure sealant bond strength to remineralized tooth surfaces: an *in vitro* study, *BMC Oral Health*, 2019, **19**, 92.

50 R. E. K. Billah, Y. Abdellaoui, Z. Anfar, G. Giácoman-Vallejos, M. Agunaou and A. Soufiane, Synthesis and characterization of chitosan/fluorapatite composites for the removal of Cr (VI) from aqueous solutions and optimized parameters, *Water Air Soil Pollut.*, 2020, **231**, 163.